ISSN 1560-3547, Regular and Chaotic Dynamics, 2010, Vol. 15, No. 6, pp. 683–701. © Pleiades Publishing, Ltd., 2010.

RESEARCH ARTICLES

Self-similarity of the Bandcount Adding Structures: Calculation by Map Replacement

V. Avrutin[1*], M. Schanz[1], and L. Gardini[2***]**

[1] *University of Stuttgart, Germany*

[2] *University of Urbino, Italy*

Received December 28, 2009; accepted February 23, 2010

Abstract—Recently it has been demonstrated that the domain of robust chaos close to the periodic domain, which is organized by the period-adding structure, contains an infinite number of interior crisis bifurcation curves. These curves form the so-called bandcount adding scenario, which determines the occurrence of multi-band chaotic attractors. The analytical calculation of the interior crisis bifurcations represents usually a quite sophisticated and cumbersome task. In this work we demonstrate that, using the map replacement approach, the bifurcation curves can be calculated much easier. Moreover, using this approach recursively, we confirm the hypothesis regarding the self-similarity of the bandcount adding structure.

MSC2000 numbers:

DOI: 10.1134/S1560354710060079

Key words:

1. INTRODUCTION

Low-dimensional chaotic attractors represent one of the central concepts in nonlinear dynamics. Therefore it seems to be a natural way to ask which bifurcation scenarios can be formed by chaotic attractors? In the case of smooth dynamical systems the chaotic domain is typically interrupted by periodic inclusions ("windows") and the rules which govern the occurrence of these inclusions are well known [1, 2]. By contrast, piecewise-smooth dynamical systems are able to demonstrate additionally so-called robust chaos. This concept, introduced in [3], refers to the situation where in some region of the parameter space (denoted as robust chaotic domain) the attractors remain chaotic under variation of parameters in some interval, and there are no periodic inclusions in this case. However, it is still possible that the geometrical structure of the attractors changes at some bifurcations within the robust chaotic domain, so that we can observe bifurcation scenarios formed by different multi-band chaotic attractors (cyclic chaotic intervals). This situation is especially typical for piecewise-smooth dynamical systems (for examples we refer to [4, 5]).

The bifurcations leading the geometrical structure of chaotic attractors to change have been known since [2, 6] (see also [7, 8]), and were later rediscovered in [9, 10]. These bifurcations, frequently denoted as crises, are typically caused by contacts of chaotic attractors with some unstable periodic orbits or their stable manifolds. These contacts may have several consequences for the dynamics. If for example the unstable periodic orbit is located at the basin boundary of the chaotic attractor, the attractor after the bifurcation is destroyed. This situation is typically denoted as a boundary crisis. If by contrast the unstable periodic orbit is located inside the closure of the basin, then the number of bands (connected components) of a multi-band chaotic attractor may change after the bifurcation. This occurs in the case of band-merging crises and typically in the case of interior crises.

[*] E-mail: Viktor.Avrutin@informatik.ini-stuttgart.de

[**] E-mail: Michael.Schanz@informatik.ini-stuttgart.de

[***] E-mail: Laura.Gardini@uniurb.it

The current state of the art in this field can be summarized as follows: specific types of crises are known, investigated from the theoretical point of view (especially it is demonstrated that all the crises, interior or exterior, represent homoclinic bifurcations [8]) and observed in experiments in several application fields. However, bifurcation structures (scenarios) formed by crisis bifurcations and determining the structure of the robust chaotic domain are still insufficiently investigated. One reason for that may be the fact that an investigation of these scenarios is not easy from the numerical point of view. In [4] some appropriate numerical algorithms were reported, through which it became possible to observe that the robust chaotic domain may be organized by complex bifurcation structures formed by crisis bifurcations.

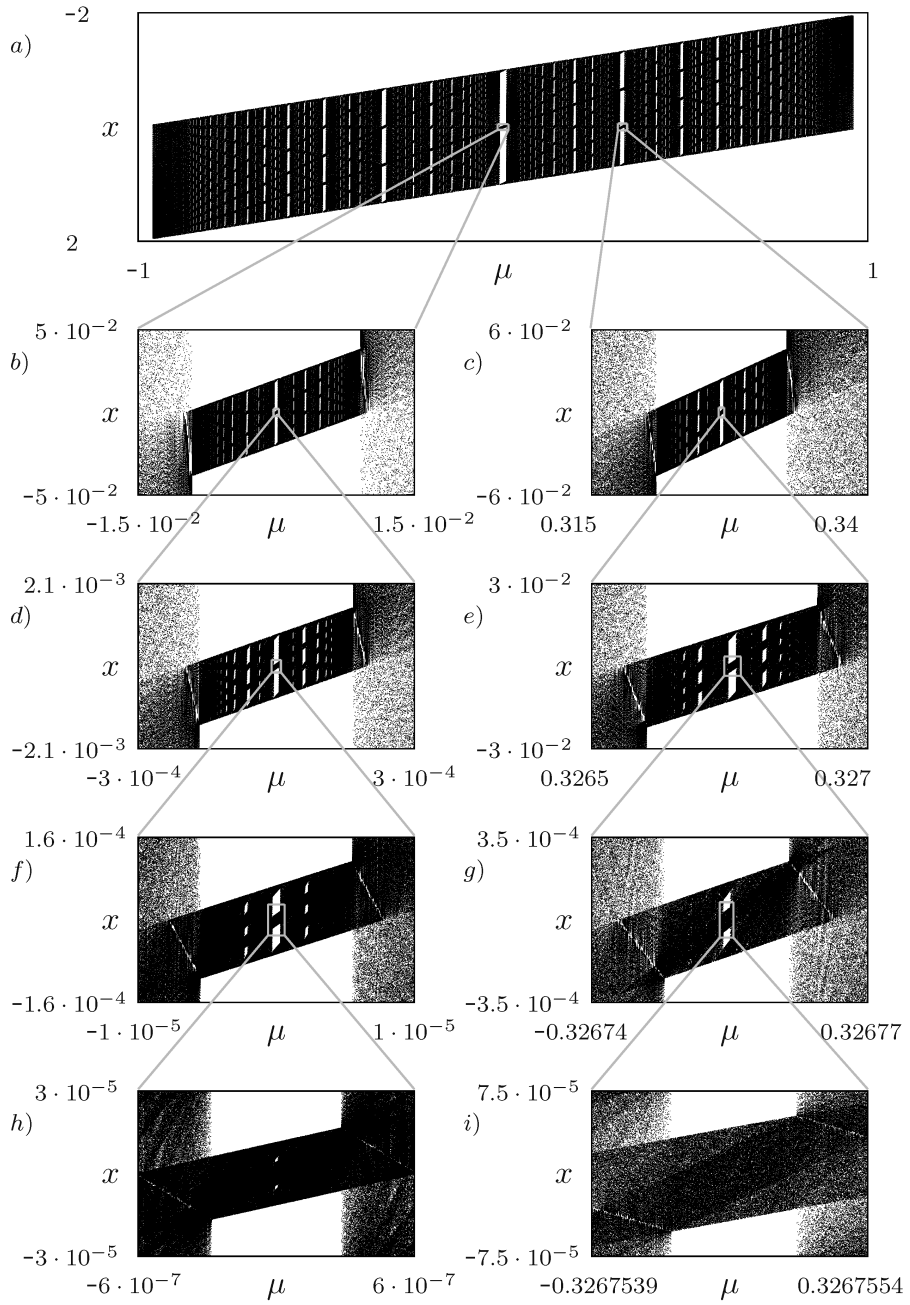

Fig. 1. Bifurcation scenario in the chaotic domain of map (1.2) for $a = 1.02$, close to the boundary with the adjacent periodic domain. Marked rectangles are shown enlarged.

One of the bifurcation structures formed by chaotic attractors only, denoted as bandcount adding scenario, was reported in [5]. It was shown that close to the boundary with the adjacent periodic domain which is organized by the Farey-tree-like period adding structure, the robust chaotic domain is organized by an infinite number of interior crisis bifurcations. One example of this structure for the piecewise-linear map (1.2), which we will introduce below, is presented in Fig. 1. It can be shown that all attractors in this figure are chaotic and no periodic inclusions are possible. In the cited work this bifurcation structure is investigated in detail both using numerical techniques and analytically. It is shown that both, the period adding and the bandcount adding structures are connected, although the bandcount adding structure is significantly more complex. The results presented lead to the hypothesis that the bandcount adding structure is self-similar.

As one can see, when enlarging a part of the bifurcation diagram shown in Fig. 1, one will find more and more nested sub-structures (see the magnifications presented in Figs. 1b and 1c and the further magnifications shown in Figs. 1d and 1e). These seem to confirm the hypothesis that the overall structure may be self-similar. However, when considering further magnifications (see Figs. 1f and 1g) one observes that the number of nested sub-structures decreases rapidly. In the example shown in Fig. 1 no sub-structures are observable in Fig. 1i. On the one hand, this may lead us to some doubts regarding the self-similarity, but on the other hand it is obvious that the self-similarity can not be verified by numerical calculations and requires an analytical description of the bifurcation structure. Although first steps in this direction are reported in the cited work, it was not clear until now how to obtain an analytical description of the bandcount adding structure which confirms or disproves its self-similarity.

Unfortunately, an analytical calculation of the crisis bifurcation curves represents a quite intricate and cumbersome task. Usually, it requires firstly to determine the unstable periodic orbit which causes the crisis bifurcation to occur, secondly to determine the boundaries of the chaotic attractor before the crisis bifurcation and eventually to find out which point of the unstable periodic orbit collides with which boundary of the chaotic attractor. These steps become more and more complex with increasing period and complexity of the unstable periodic orbit and of the chaotic intervals.

A significant simplification of the described procedure turns out to be possible using the map replacement approach described in [11]. This approach allows a very efficient calculation of periodic orbits as well as their bifurcations, and goes back to the ideas presented by Leonov [12–14] almost 50 years ago. The idea of this approach is based on the following observation. It is an obvious way to consider instead of an n-periodic orbit the fixed points of the corresponding nth iterated function. This allows a unified and typically very descriptive reasoning. Unfortunately, from the point of view of computational effort, the calculation of the nth iterated function for large n is in general a complicated task. However, for the piecewise-linear map

$$x_{n+1} = f(x_n) = \begin{cases} f_\ell(x_n) = a_\ell x_n + \mu_\ell \,\text{if}\, x_n < 0 \\ f_r(x_n) = a_r x_n + \mu_r \,\text{if}\, x_n > 0 \end{cases} \tag{1.1}$$

which we consider in the following, we can make use of the fact that the iterated functions remain piecewise-linear. In general, the map replacement approach works for any system where the iterated function has the same functional form (form invariance) as the original system function. Let us now assume that the n-periodic orbit $\mathcal{O}_\rho$, for which we are going to calculate the bifurcation curves, corresponds to the symbolic sequence ρ (hereby we write the symbols $\mathcal{L}$ and $\mathcal{R}$ if for a point x_i of a periodic orbit holds $x_i < 0$ and $x_i > 0$, respectively). Let us further assume that the sequence ρ results from a different (shorter) sequence σ by replacement of all symbols $\mathcal{L}$ with a syllable ϖ_ℓ and all symbols $\mathcal{R}$ with a syllable ϖ_r. For example, for $\rho = \mathcal{LRRLRLL}$ and $\sigma = \mathcal{LRR}$ we have $\varpi_\ell = \mathcal{LR}$ and $\varpi_r = \mathcal{RL}$. Under these (and some more, see [11]) assumptions it is possible to define a composite map consisting of the linear functions iterated according to the sequences ϖ_ℓ and ϖ_r. For this composite map we can adjust its parameters (which depend on the parameters of the original system function f) in such a way that its shape coincides exactly with the shape of the original map. This can be done especially at the bifurcation points, so we can transfer the bifurcation curves obtained for the original map and the orbit $\mathcal{O}_\sigma$ to the same orbit in the composite map. Moreover, since the orbit $\mathcal{O}_\sigma$ for the composite map corresponds to the orbit $\mathcal{O}_\rho$ for the original map, from the bifurcation curves for the orbit $\mathcal{O}_\sigma$ we obtain the bifurcation curves for the orbit $\mathcal{O}_\rho$.

The main idea of the map replacement approach is to calculate the bifurcation curves for a periodic orbit with a large period not by using the fixed points of the corresponding iterated function but by using a periodic orbit with a preferably much smaller period, and a map which is composed in an appropriate way from "not too high"-iterated functions. For example, to calculate the bifurcation curves of the period-6 orbit $\mathcal{O}_{\mathcal{LRRLRL}}$ we consider not the fixed points of the 6th iterated function but the period-3 orbit $\mathcal{O}_{\mathcal{LRR}}$ and the composite map consisting of the two linear functions $f_{\ell r} = f_r \circ f_\ell$ and $f_{r\ell} = f_\ell \circ f_r$ which represent parts of the second iterated of f. In the original works by Leonov [12–14] as well as in [11] the map replacement approach is used for the calculation of border-collision bifurcations. However, the approach is not restricted to this type of bifurcations. In the current work we demonstrate that this approach is also useful for the analytical calculation of crisis bifurcations. Therefore, the current work represents a synthesis of two preliminary works, namely [5] where the bandcount adding structure was introduced and [11] where the map replacement approach was reported. In conformity with the cited works, we use for the graphical representation of the results obtained for (1.1) the map

$$x_{n+1} = f(x_n) \begin{cases} f_\ell(x_n) = ax_n + \mu + 1 \text{ if } x_n < 0 \\ f_r(x_n) = ax_n + \mu - 1 \text{ if } x_n > 0 \end{cases} \tag{1.2}$$

which has only two parameters. Obviously, using the substitution $a_\ell = a,\ a_r = a,\ \mu_\ell = \mu + 1$, $\mu_r = \mu - 1$ the results obtained for (1.1) will be transformed into corresponding results for (1.2). Note that for any period-n orbit of system (1.2) the eigenvalue is given by a^n, and hence no stable periodic orbits are possible in system (1.2) for $a > 1$.

The work presented below is organized as follows. First, in Section 2 we discuss a motivating example and demonstrate why the map replacement approach, which was initially developed for the calculation of border collision bifurcations, can also be applied for the calculation of crisis bifurcation curves. Then, in Section 3 we discuss the main structure of the domain of robust chaos in system (1.2). Hereby all calculation steps are performed for the general map (1.1) and are therefore directly applicable for any other 1D piecewise-linear map of particular interest. As a next step, in Section 4 and Section 5 we investigate self-similar substructures in the robust chaotic domain. Whereas in [5], only a few of their substructures were reported, by applying the map replacement approach we are able to calculate them analytically up to a precision level which is currently far beyond any possibilities of numerical calculations.

2. MOTIVATING EXAMPLE

Let us consider here a motivating example by using the map (1.2) at $\mu = 0$ for which (as we shall see in the next section) a cycle of period 2 always exists. The 2-cycle is stable for $a < 1$ and unstable for $a > 1$, where we have bounded dynamics in chaotic intervals up to $a = 2$. In order to appreciate the whole self-similar structure we shall comment on decreasing the parameter a, starting from $a > 2$ (see Fig 2a). The situation at $a = 2$ corresponds to the homoclinic bifurcation of the unstable fixed points P_+^* and P_-^* of f. Fig. 2b shows the map f at $a = 2$, when we have $f_\ell(0) = P_+^*$ and $f_r(0) = P_-^*$. The map f is invariant in the interval $I = [f_r(0), f_\ell(0)]$, and in this invariant interval the map is the well-known *full shift-map*. Thus f is fully chaotic inside I. The properties of the shift map are well known: any point in I has two distinct rank-one preimages, and the two inverses are such that $f_\ell^{-1}(I) = I$ and $f_r^{-1}(I) = I$ (thus $f^{-1}(I) = I$ also holds). All possible cycles exist and are homoclinic, which is very simple to prove. Consider for example the second iterate f^2 also shown in Fig. 2b. It consists of four pieces defined by the functions f_ℓ^2, $f_r \circ f_\ell$, $f_\ell \circ f_r$, f_r^2, and the discontinuity points of f^2 are given by the point $x = 0$ and the two rank-1 preimages of this point. As one can see in Fig. 2b, all four pieces together take all the values in I, and clearly the same property occurs for the iterates f^{2k} for any $k > 2$. This is true not only for the integer 2: the same holds for any other integer n. For example, the function f^3 consists of $8 = 2^3$ branches (the discontinuity points between the branches are given by the point $x = 0$ and its rank-1 and -2 preimages), all of them together take all the values in I.

Notice that outside I the trajectories are diverging (as the fixed points are unstable). Thus for $a > 2$ (see Fig. 2a) the generic trajectory is divergent: the interval I is no longer invariant and the

invariant set inside I is a chaotic repellor Λ, with periodic points of any period and any symbolic sequence constructed as described in Section 3, Section 4 and Section 5.

Along the path ($\mu = 0$) here chosen, we know that a 2-cycle always exists (stable or unstable) thus the map which interests us, as the parameter a is decreased, is the second iterate f^2 which clearly has two fixed points corresponding to the 2-cycle. Decreasing the parameter from $a = 2$ (when all the cycles are homoclinic) we have that the 2-cycle persists homoclinic in some interval, say for $a_2 < a < 2$ (where, as we shall see, $a_2 = 2^{1/2} = 1.4142...$). For a value of a in this range the map f^2 has the interval bounded by the limiting values of the function f^2 in $x = 0$, namely $J = [f_r \circ f_\ell(0), f_\ell \circ f_r(0)]$ which includes the unstable points of the 2-cycle (see Fig. 2c at $a = 1.7$), and thus J it is not invariant. Locally the map f^2 behaves on J like the map f on I for $a > 2$. However, while the map f for $a > 2$ has no other branches and no feed-back mechanism, here the map f^2 has other branches, so that a trajectory exiting from J will always be confined in $I \supset J$ as the map f is invariant in I. Also notice that f^2 in the interval bounded by the 2-cycle behaves like the map f for $a > 2$ between the two unstable fixed points, thus a chaotic set Λ exists which is here invariant for f^2 but being $f^2(J) \supset J$ in a few steps we have $f^{2n}(J) = I$ and thus the map is chaotic in the whole interval I (i.e. chaotic bands cannot exist). Notice that for $a < 2$ the chaos in the interval I is no longer a full shift for f. In fact, while the points of the interval J still have two distinct rank-1 preimages in I, the points of the intervals $I \setminus J$ (see Fig. 2c) have only one rank-one preimage inside I and the other one is external to I (inside the basin of attraction of the absorbing interval I). Clearly repelling periodic points are also in the portions $I \setminus J$. However, the periodic points belonging to $I \setminus J$ can be homoclinic only on one side (as the other has a preimage outside I). Thus, in this interval $a_2 < a < 2$ the map f is chaotic in I, and not only the 2-cycle is homoclinic: due to the shape of f^2 in J we have that all the fixed points of $(f^2)^k$ also belong to homoclinic cycles of period 2^k.

It is clear that as a is decreased the homoclinic bifurcation of the 2-cycle is approached and at $a = a_2 = 2^{1/2}$ locally, for the map f^2 in J, we are in the same situation as for the map f at $a = 2$. Comparing Figs. 2d and 2a one can clearly see that f^2 in J is a full shift. Hence, we can repeat for f^2 the same properties stated above for f at $a = 2$. The boundary of J consists of two unstable fixed points. However now outside J we have not divergence, instead the two intervals of $I \setminus J$ are now two cyclic chaotic intervals. The invariant interval I of f consists of two invariant chaotic sets: the interval J and two cyclic chaotic intervals in $I \setminus J$.

For $a < a_2$ (exactly for $a_4 < a < a_2$, $a_4 = 2^{1/4} = 1.1892...$) we can repeat the same reasoning. Now the maps f^2 and f^4 play the same role as the maps f and f^2 in the previous arguments. In Figs. 2e and 2f for $a = 1.2$ we can see that f^2 is invariant in an interval $I' = J$ and f^4 has two unstable fixed points inside $J' = [f_\ell \circ f_r^2 \circ f_\ell(0), f_r \circ f_\ell^2 \circ f_r(0)]$ (that means, J' is bounded by the limiting values of the function f^4 in $x = 0$) which are homoclinic. For the map f the points of the 2-cycle are no longer homoclinic. In fact, they no longer belong to a chaotic interval, and are outside the invariant intervals, which are detected via f^2. The invariant intervals are given by I' and its images by f (thus in total three intervals because I includes the discontinuity point). The complementary sets has "two holes" between the cyclic chaotic intervals, which include the points of the unstable 2-cycle.

As the parameter a is decreased we can see all the self-similar bifurcations (the self similarity is clearly in the shapes of the maps inside the intervals I' and J'). And this can be repeated for any k, dealing with all the homoclinic bifurcations of the cycles of period 2^k which, starting from $a = 2$, we know all exist and are all homoclinic (while in $a = 1$ no one is homoclinic).

Let us now reconsider the similarity between the roles of the function f at the point $a = 2$ and the function f^2 at the point $a = 2^{1/2}$. Suppose, we have a description of the bifurcation which occurs in map (2) at $a = 2$, in terms of the coefficients of the general map (1), that means a_ℓ, μ_ℓ, a_r, μ_r,. Then the same description is also valid for the bifurcation which occurs in map (2) at $a = 2^{1/2}$ in terms of the coefficients of the second iterated of the general map (1). The relevant two branches of the second iterated are $f_{\ell r} = f_r \circ f_\ell$ and $f_{r\ell} = f_\ell \circ f_r$, and their coefficients $a_{\ell r}$, $\mu_{\ell r}$, $a_{r\ell}$, $\mu_{r\ell}$, can be calculated easily (see Section 4). That means, we can proceed as follows. Fist, we calculate the analytical expressions for the bifurcation curves caused in the original map by

the period-2 orbit $\mathcal{O}_{\mathcal{LR}}$. Then, in these expressions we replace the coefficients a_ℓ, μ_ℓ, a_r, μ_r by the composite coefficients $a_{\ell r}$, $\mu_{\ell r}$, $a_{r\ell}$, $\mu_{r\ell}$. The resulting expressions represent the bifurcations of the period-2 orbit for the function f^2 and consequently the bifurcations of the period-4 orbit for the original function f.

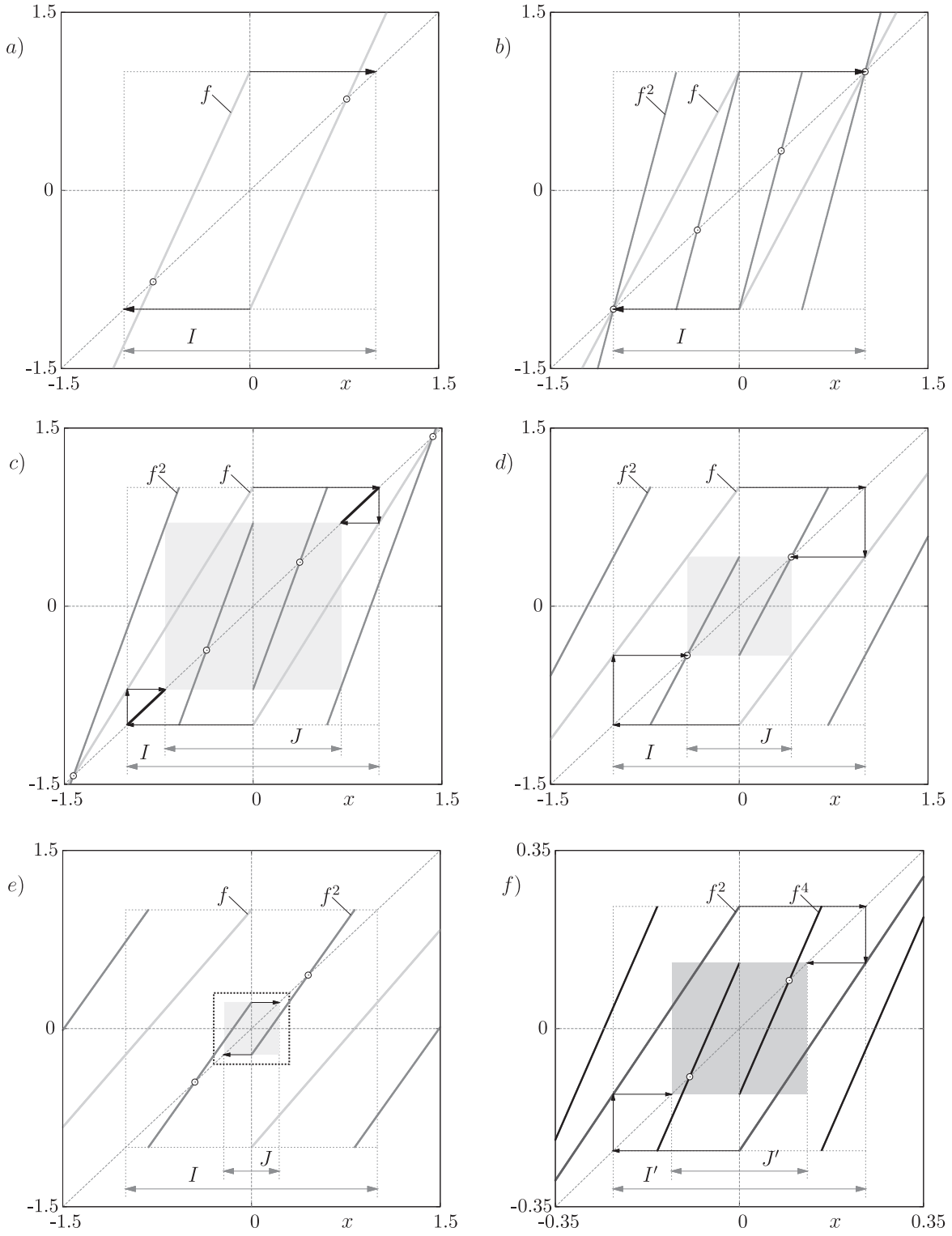

Fig. 2. Evolution of the system function of map (1.2) for $\mu = 0$ and a decreasing. a) $a = 2.2$, b) $a = 2$, c) $a = 1.7$ d) $a = 2^{1/2}$, e,f) $a = 1.22$. The square marked dotted in e) is shown enlarged in f).

3. OVERALL BANDCOUNT ADDING

It is shown in [5] that the domain of robust chaos in system (1.2) is structured by the bandcount adding scenario. As system (1.2) represents a special case of system (1.1), it is clear that system (1.1) shows this scenario as well. Within this scenario for system (1.2), each periodic orbit which is stable in the periodic domain and becomes unstable at the boundary $a = 1$, is involved in two interior crisis bifurcations. For an orbit $\mathcal{O}_\sigma$ the curves in the parameter space of these bifurcations confine the region $\mathcal{Q}_\sigma^{|\sigma|+1}$ where chaotic attractors consist of $|\sigma| + 1$ bands whereby $|\sigma|$ denotes the length of the symbolic sequence $|\sigma|$. As the orbits within the stable, or periodic, domain are organized by the period adding structure, the multi-band regions $\mathcal{Q}_\sigma^{|\sigma|+1}$ are organized similarly. As one can see in Fig. 3, the chaotic domain is linked to the periodic domain: each periodic region for $a < 1$ is continued for $a > 1$ with a corresponding multi-band region.

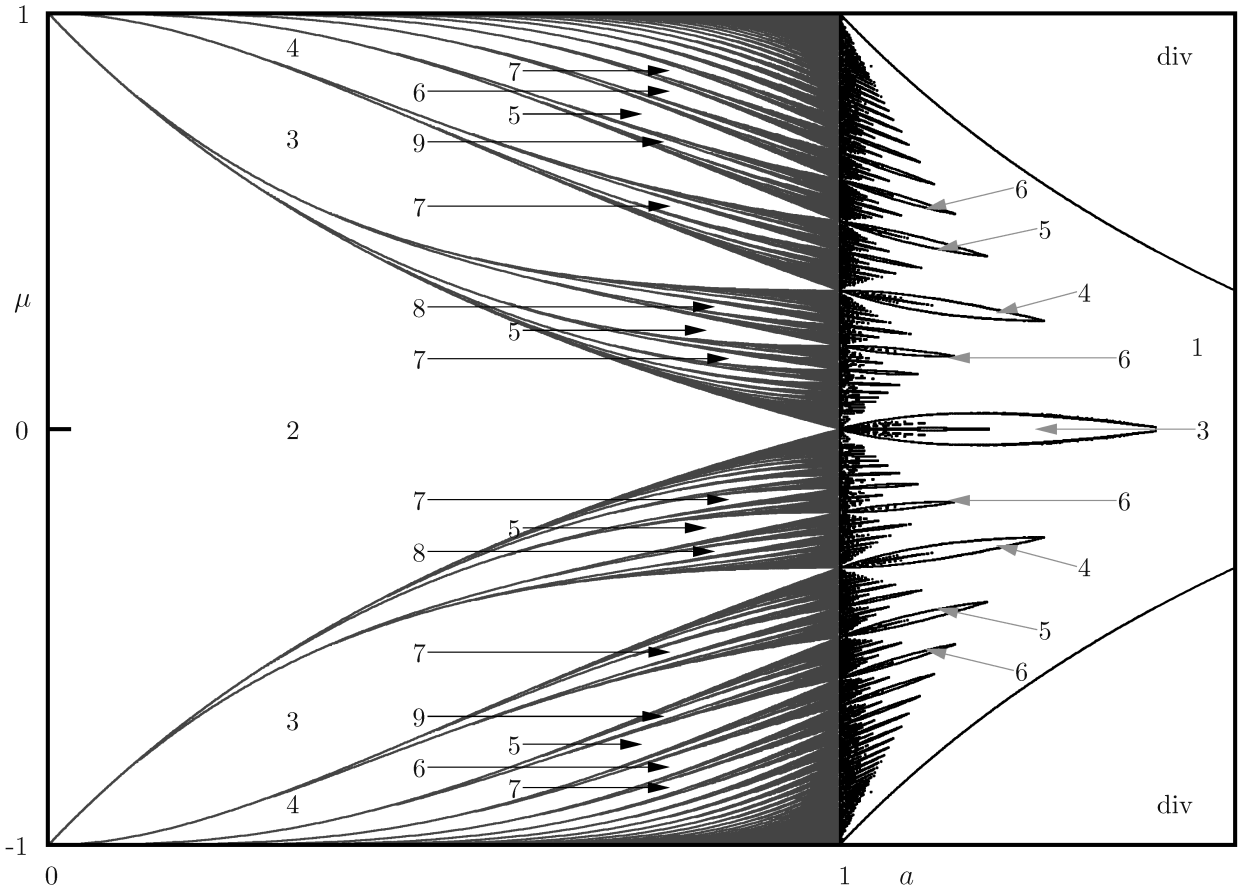

Fig. 3. Numerically calculated bifurcation structure of map (1.2). For $a \leqslant 1$ the dynamics is periodic, some of the periods are marked. For $a > 1$ the dynamics is chaotic, some of the bandcounts are marked.

An analytical calculation of the interior crisis bifurcation curves is presented in [5] mainly for the basic orbits, that means for orbits corresponding to the two families of symbolic sequences

$$\{\mathcal{LR}^{n_1} \mid n_1 > 0\} \quad \text{and} \quad \{\mathcal{RL}^{n_1} \mid n_1 > 0\} \tag{3.1}$$

As shown in the cited work, the interior crisis bifurcation curves $\eta^{\ell/r}_{\mathcal{LR}^{n_1}}$ and $\eta^{\ell/r}_{\mathcal{RL}^{n_1}}$ corresponding to these sequences, confine the regions $\mathcal{Q}^{n_1+2}_{\mathcal{LR}^{n_1}}$ and $\mathcal{Q}^{n_1+2}_{\mathcal{RL}^{n_1}}$ of $(n_1 + 2)$-band chaotic attractors. As an example, for the calculation of the curves $\eta^{\ell/r}_{\mathcal{LR}^{n_1}}$ the conditions $x^{\mathcal{LR}^n}_{0/n} = x^{ko}_{r/\ell}$ can be used where the values $x^{ko}_\ell = f_{\ell r \ell^{n-1}}(0)$ and $x^{ko}_r = f_{r\ell r^{n-1}}(0)$ define the boundaries of the chaotic attractors with

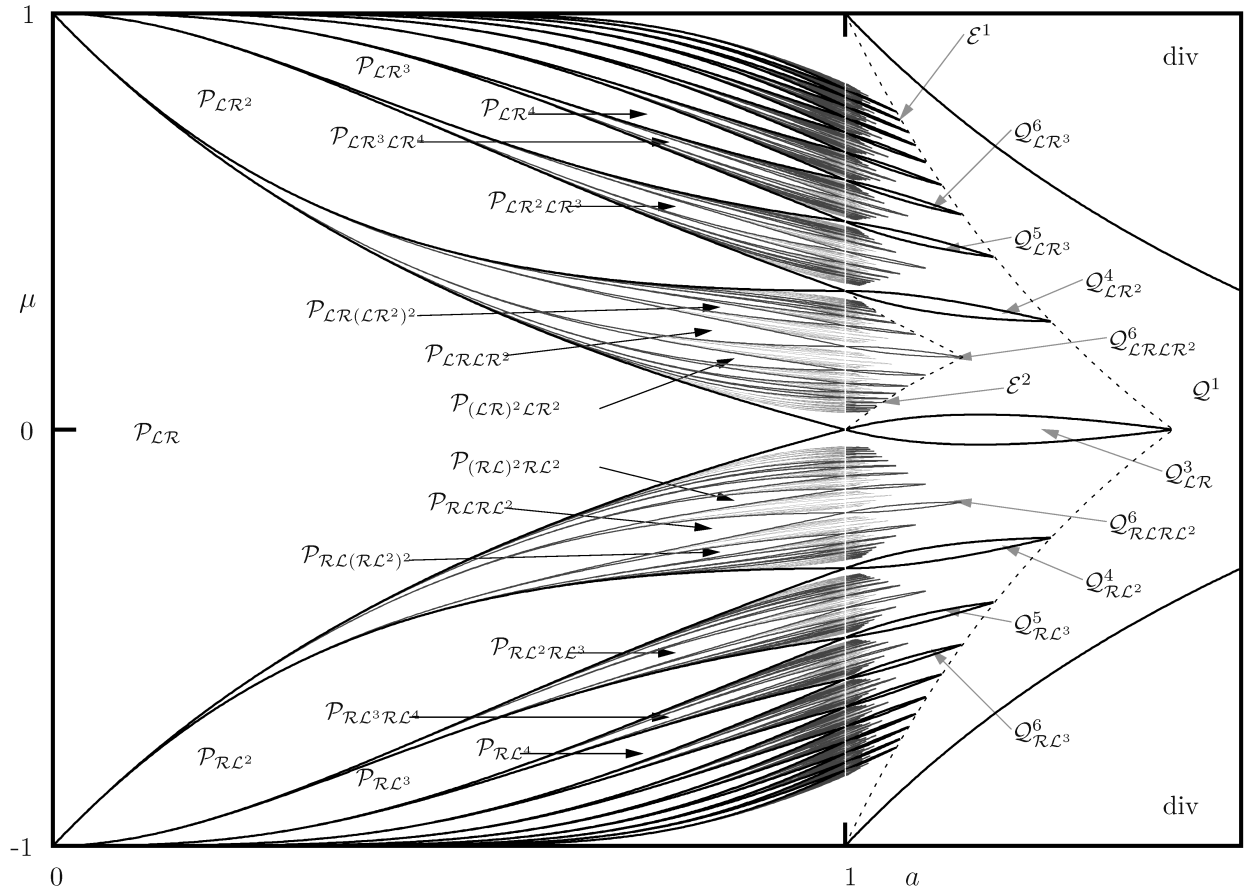

Fig. 4. Analytically calculated period adding and bandcount adding structures of map (1.2). In both domains, the periodic and the chaotic one, the bifurcation curves corresponding to complexity level one, two and three are shown as black, dark gray and light gray curves, respectively. They are plotted for $n_1 = 1..12$, $n_2 = 1..10$, $n_3 = 1..5$.

which the points $x^{\mathcal{LR}^n}_{0/n}$ of the unstable periodic orbits collide. From this conditions we obtain

$$\begin{aligned}
\eta^{\ell}_{\mathcal{LR}^{n_1}} &= \left\{ (a_\ell, a_r, \mu_\ell, \mu_r) \;\middle|\; \frac{\mu_\ell}{\mu_r} = -\frac{a_\ell a_r^{n_1}(a_\ell a_r - a_\ell + 1) - 2a_\ell a_r + a_r + a_\ell - 1}{(a_r-1)^2 + a_\ell a^{n_1}(a_r - 1)} \right\} \\
\eta^{r}_{\mathcal{LR}^{n_1}} &= \left\{ (a_\ell, a_r, \mu_\ell, \mu_r) \;\middle|\; \frac{\mu_\ell}{\mu_r} = \frac{a_\ell a_r^{n_1+1} - a_r - a_\ell + 1}{(a_r-1)^2 - a_\ell a_r^{n_1+1}(a_r - 1)} \right\}
\end{aligned} \tag{3.2}$$

The bifurcation curves $\eta^{\ell/r}_{\mathcal{RL}^{n_1}}$ can be obtained analogously. In principle, the crisis bifurcation curves for other orbits can be calculated in a similar way. As these calculations represent a quite cumbersome task, it was not done in the cited work. As we will demonstrate, using the map replacement approach, the calculations become a comparably easy task.

Recall that according to Leonov the families of orbits $\mathcal{O}_{\mathcal{LR}^{n_1}}$ and $\mathcal{O}_{\mathcal{RL}^{n_1}}$ form the first level of complexity or complexity level one of the period adding structure. The regions located between the regions of complexity level one belong to the complexity level two, whereby the corresponding symbolic sequences form the families

$$\{\mathcal{LR}^{n_2}(\mathcal{RLR}^{n_2})^{n_1} \mid n_1 > 0, n_2 > 0\}, \tag{3.3}$$

$$\{\mathcal{RLR}^{n_2}(\mathcal{LR}^{n_2})^{n_1} \mid n_1 > 0, n_2 > 0\}, \tag{3.4}$$

$$\{\mathcal{RL}^{n_2}(\mathcal{LRL}^{n_2})^{n_1} \mid n_1 > 0, n_2 > 0\}, \tag{3.5}$$

$$\{\mathcal{LRL}^{n_2}(\mathcal{RL}^{n_2})^{n_1} \mid n_1 > 0, n_2 > 0\} \tag{3.6}$$

and can be obtained from the sequences of complexity level one using the replacements

$$\begin{cases} \mathcal{L} \to \mathcal{L}\mathcal{R}^{n_2} \\ \mathcal{R} \to \mathcal{R}\mathcal{L}\mathcal{R}^{n_2} \end{cases} \tag{3.7}$$

$$\begin{cases} \mathcal{L} \to \mathcal{L}\mathcal{R}\mathcal{L}^{n_2} \\ \mathcal{R} \to \mathcal{R}\mathcal{L}^{n_2} \end{cases} \tag{3.8}$$

It was already demonstrated in [5] that the calculation of the border-collision bifurcations involving orbits of complexity level two can be done in the following way: firstly we calculate the coefficients $a_{\ell r^n}$, $\mu_{\ell r^n}$, $a_{r\ell r^n}$, $\mu_{r\ell r^n}$ of the composite function

$$x_{n+1} = \begin{cases} f_{\ell r^n}(x_n) &= a_{\ell r^n} x_n + \mu_{\ell r^n} \quad \text{if } x_n < 0 \\ f_{r\ell r^n}(x_n) &= a_{r\ell r^n} x_n + \mu_{r\ell r^n} \text{ if } x_n > 0 \end{cases} \tag{3.9}$$

defined as the coefficients of the following iterated functions

$$\begin{aligned} f_{\ell r^n}(x) &= f_r \circ \cdots \circ f_r \circ f_\ell(x) \\ &= \underbrace{a_\ell a_r^n}_{a_{\ell r^n}} x + \underbrace{\frac{-a_r^n \mu_\ell + a_r^{n+1}\mu_\ell + \mu_r\, a_r^n - \mu_r}{-1 + a_r}}_{\mu_{\ell r^n}} \end{aligned} \tag{3.10}$$

$$\begin{aligned} f_{r\ell r^n}(x) = {} & f_r \circ \cdots \circ f_r \circ f_\ell \circ f_r(x) = \underbrace{a_\ell a_r^{n+1}}_{a_{r\ell r^n}} x + \\ & \underbrace{\frac{(a_r^{n+1}a_\ell - a_r^n a_\ell + a_r^n - 1)\mu_r + (a_r^{n+1} - a_r^n)\mu_\ell}{-1 + a_r}}_{\mu_{r\ell r^n}} \end{aligned} \tag{3.11}$$

(the coefficients $a_{r\ell^n}$, $\mu_{r\ell^n}$, $a_{\ell r\ell^n}$, $\mu_{\ell r\ell^n}$ are defined analogously exchanging ℓ and r). Secondly, these coefficients will be inserted in the equations of the border-collision bifurcations of the orbits of complexity level one instead of the coefficients a_ℓ, μ_ℓ, a_r, μ_r. As a consequence, the composite map (3.9) demonstrates in this case the same behavior as the original map (1.1) at the corresponding parameter values, that means undergoes the same bifurcations. Eventually we resolve the obtained expressions with respect to the original coefficients a_ℓ, μ_ℓ, a_r, μ_r and get the border-collision bifurcations of the orbits of complexity level two for the original map (1.1).

Repeating the same procedure one more time we calculate the crisis bifurcation curves corresponding to orbits of complexity level three. As there are two replacements (3.7) and (3.8), the number of families is doubled with each complexity level. Hence, in complexity level three there are $2^3 = 8$ families, the first four of them are

$$\{\mathcal{L}\mathcal{R}^{n_3}(\mathcal{R}\mathcal{L}\mathcal{R}^{n_3})^{n_2}((\mathcal{L}\mathcal{R}^{n_3}(\mathcal{R}\mathcal{L}\mathcal{R}^{n_3})^{n_2+1})^{n_1} \mid n_1 > 0, n_2 > 0, n_3 > 0\} \tag{3.12}$$

$$\{\mathcal{L}\mathcal{R}^{n_3}(\mathcal{R}\mathcal{L}\mathcal{R}^{n_3})^{n_2+1}((\mathcal{L}\mathcal{R}^{n_3})(\mathcal{R}\mathcal{L}\mathcal{R}^{n_3})^{n_2})^{n_1} \mid n_1 > 0, n_2 > 0, n_3 > 0\} \tag{3.13}$$

$$\{\mathcal{R}\mathcal{L}\mathcal{R}^{n_3}(\mathcal{L}\mathcal{R}^{n_3})^{n_2+1}((\mathcal{R}\mathcal{L}\mathcal{R}^{n_3})(\mathcal{L}\mathcal{R}^{n_3})^{n_2})^{n_1} \mid n_1 > 0, n_2 > 0, n_3 > 0\} \tag{3.14}$$

$$\{\mathcal{R}\mathcal{L}\mathcal{R}^{n_3}(\mathcal{L}\mathcal{R}^{n_3})^{n_2}((\mathcal{R}\mathcal{L}\mathcal{R}^{n_3})(\mathcal{L}\mathcal{R}^{n_3})^{n_2+1})^{n_1} \mid n_1 > 0, n_2 > 0, n_3 > 0\} \tag{3.15}$$

and the remaining four families result from the families listed above by simply exchanging $\mathcal{L}$ and $\mathcal{R}$. This calculation procedure can be continued recursively, that means using the 2^i families of bifurcation curves in complexity level i and the two replacements (3.7), (3.8) we obtain the 2^{i+1} families of bifurcation curves in complexity level $i+1$. The results of the calculation for the first three levels of complexity for system (1.2) can be seen in Fig. 4 for $a < 1$.

Exactly the same steps can be performed for the calculation of the crisis bifurcation curves. In this case the replacement coefficients $a_{\ell r^n}$, $\mu_{\ell r^n}$, $a_{r\ell r^n}$, $\mu_{r\ell r^n}$ will be inserted in the equations for $\eta^{\ell/r}_{\mathcal{L}\mathcal{R}^{n_1}}$ and $\eta^{\ell/r}_{\mathcal{R}\mathcal{L}^{n_1}}$ leading to the four families of crisis bifurcation curves $\eta^{\ell/r}_{\mathcal{L}\mathcal{R}^{n_2}(\mathcal{R}\mathcal{L}\mathcal{R}^{n_2})^{n_1}}$, $\eta^{\ell/r}_{\mathcal{R}\mathcal{L}\mathcal{R}^{n_2}(\mathcal{L}\mathcal{R}^{n_2})^{n_1}}$, $\eta^{\ell/r}_{\mathcal{R}\mathcal{L}^{n_2}(\mathcal{R}\mathcal{L}\mathcal{R}^{n_2})^{n_1}}$, $\eta^{\ell/r}_{\mathcal{L}\mathcal{R}\mathcal{L}^{n_2}(\mathcal{R}\mathcal{L}^{n_2})^{n_1}}$ involving orbits of complexity level two. The calculation results for system (1.2) for the first three levels of complexity can be seen in Fig. 4 for $a > 1$.

Let us now consider the described procedure from a different point of view. From the steps discussed above it becomes clear, that each application of the replacements (3.7) and (3.8) for any fixed n represents some kind of area-to-area mapping in the parameter space. Let us consider for example the area bounded by the line $a = 1$ and the envelope $\mathcal{E}^1$ shown in Fig. 4. For $n = 1$ the calculation according to the replacement (3.7) maps each bifurcation curve located in this area onto the small part of this area bounded by the line $a = 1$ and the envelope $\mathcal{E}^2$ marked in Fig. 4. Hereby the bifurcation curves of complexity level one will be mapped onto the curves of complexity level two, the curves of complexity level two will be mapped onto the curves of complexity level three, and in general the curves of complexity level i will be mapped onto the curves of complexity level $i + 1$. This area-to-area mapping represents a strong evidence for the self-similarity of the overall bandcount adding structure.

4. BANDCOUNT DOUBLING INSIDE $\mathcal{Q}^3_{\mathcal{LR}}$

The overall bandcount adding scenario is not the only bifurcation scenario occurring in system (1.1) within the domain of robust chaos. It was demonstrated in [5] for system (1.2) that along the middle curve of each region involved in the overall bandcount adding structure there exists an infinite bandcount doubling cascade. As an example for the first steps of this cascade, let us consider the bifurcation scenario presented in Fig. 5. This scenario occurs along the line $\mu = 0$ which represents the middle line of the region $\mathcal{Q}^3_{\mathcal{LR}}$ (see Eqs. 3.2 for $n_1 = 1$). In Fig. 5a the boundary of this region can be clearly seen, given by the crisis bifurcation where the one-band attractor becomes a three-band attractor. Also the next bifurcation in this cascade which leads from a three-band to a seven-band attractor is clearly visible in Fig. 5a. As the magnification in Fig. 5b shows, in the region of the seven-band attractor the region of 15-band attractor is nested, and so on. As illustrated by a series of magnifications shown in Figs. 5c– 5f, the sequence of bandcounts in the nested regions is 3, 7, 15, 31, 63, ... As shown in [5], this cascade represents an infinite sequence of nested regions confined by interior crisis bifurcation curves involving unstable periodic orbits with doubled periods. In general, the bandcounts in the cascade occurring within the region $\mathcal{Q}_\sigma^{|\sigma|+1}$ are given by

$$\mathcal{K}_i^n = 1 + |\sigma| \cdot \sum_{k=0}^{i-1} 2^k = 1 + |\sigma|(2^i - 1) = |\sigma| + 1, 3|\sigma| + 1, 7|\sigma| + 1, \dots \tag{4.1}$$

and are caused by unstable periodic orbits with periods $2^k|\sigma|$. In the special case of the cascade within the region $\mathcal{Q}^3_{\mathcal{LR}}$, that means for $|\sigma| = 2$, Eq. (4.1) implies that the bandcounts in the bandcount doubling cascade are 3, 7, 15, 31, 63,..., whereby the corresponding crisis bifurcations are caused by the orbits with periods 2, 4, 8, 16, 32. Note that the first steps of this cascade are shown not only in Fig. 5 but also in Figs. 1b, 1d, 1f, and 1h. Similarly, within the region $\mathcal{Q}^4_{\mathcal{LR}^2}$, that means for $|\sigma| = 3$, the bandcount doubling cascade is caused by the orbits with periods 3, 6, 12, 24... and the resulting bandcounts are 4, 10, 22, 46..., as illustrated in Figs. 1c, 1e, 1g, and 1i. Note that for increasing bandcounts the size of specific bands decreases rapidly, so that numerical observations become an intricate task.

For the analytical description of the bandcount doubling cascades it is necessary to determine the symbolic sequences of the orbits undergoing the crisis bifurcations. In [5] the rules for the creation of these sequences were reported. Especially, within the region $\mathcal{Q}^3_{\mathcal{LR}}$ these sequences are given by

$$\begin{aligned}
\sigma_2 &= \mathcal{LR}^2\mathcal{L}, \\
\sigma_3 &= \mathcal{LR}^2\mathcal{LRL}^2\mathcal{R}, \\
\sigma_4 &= \mathcal{LR}^2\mathcal{LRL}^2\mathcal{R}^2\mathcal{L}^2\mathcal{RLR}^2\mathcal{L}, \\
\sigma_5 &= \mathcal{LR}^2\mathcal{LRL}^2\mathcal{R}^2\mathcal{L}^2\mathcal{RLR}^2\mathcal{LRL}^2\mathcal{RLR}^2\mathcal{L}^2\mathcal{R}^2\mathcal{LRL}^2\mathcal{R}, \\
&\dots
\end{aligned} \tag{4.2}$$

Remarkably, in the general case (for an arbitrary σ) the creation rule reported in [5] for the symbolic sequences in the bandcount doubling cascade nested in $\mathcal{Q}_\sigma^{|\sigma|+1}$ represents a 2D mapping

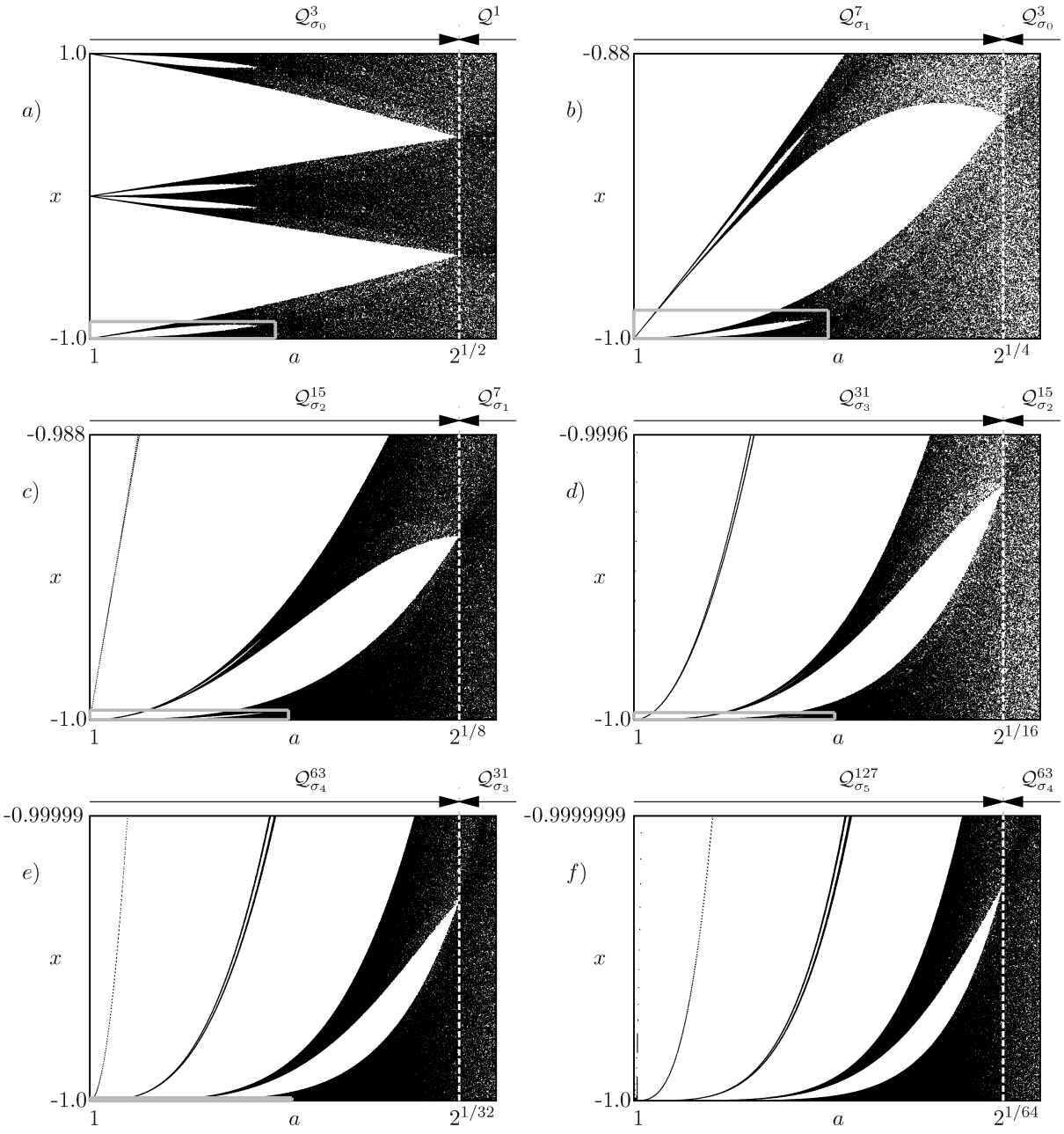

Fig. 5. Bifurcation structure along the line $\mu = 0$ forming the first steps of the bandcount doubling cascade within the region $\mathcal{Q}^3_{\mathcal{LR}}$ in system (1.2). Rectangles marked in figures *a*–*e* are shown enlarged in figures *b*–*f*, respectively.

in the space of symbolic sequences. However, it turns out that in the special case of the structures nested in $\mathcal{Q}^3_{\mathcal{LR}}$ these sequences can also be created by repeated application of the following simple replacement

$$\mathcal{L} \to \mathcal{LR}, \qquad \mathcal{R} \to \mathcal{RL} \tag{4.3}$$

starting with $\sigma_1 = \mathcal{LR}$. This allows us to calculate all bifurcation curves forming the bandcount doubling cascade nested in $\mathcal{Q}^3_{\mathcal{LR}}$ using the map replacement approach and the following recursive

replacement scheme:

$$\eta_{\sigma_i}^{\ell/r} \xrightarrow[\substack{a_\ell \mapsto a_{\ell r}\ \ a_r \mapsto a_{r\ell} \\ \mu_\ell \mapsto \mu_{\ell r}\ \ \mu_r \mapsto \mu_{r\ell}}]{\substack{\mathcal{L} \mapsto \mathcal{L}\mathcal{R} \\ \mathcal{R} \mapsto \mathcal{R}\mathcal{L}}} \eta_{\sigma_{i+1}}^{\ell/r} \tag{4.4}$$

where the replacement coefficients are defined as follows:

$$\begin{aligned} f_{\ell r}(x) &= f_r \circ f_\ell(x) = \underbrace{a_\ell a_r}_{a_{\ell r}} x + \underbrace{a_r \mu_\ell + \mu_r}_{\mu_{\ell r}} \\ f_{r\ell}(x) &= f_\ell \circ f_r(x) = \underbrace{a_\ell a_r}_{a_{r\ell}} x + \underbrace{a_\ell \mu_r + \mu_\ell}_{\mu_{r\ell}} \end{aligned} \tag{4.5}$$

Following Eq. (4.4) we substitute the coefficients $a_{\ell r}$, $\mu_{\ell r}$, $a_{r\ell}$, $\mu_{r\ell}$ into the equations for the interior crisis bifurcation curves involving the orbit $\mathcal{O}_{\mathcal{L}\mathcal{R}}$ (given by Eq. (3.2) for $n_1 = 1$) and obtain the interior crisis bifurcation curves $\eta_{\mathcal{L}\mathcal{R}^2\mathcal{L}}^{\ell/r}$ caused by the orbit $\mathcal{O}_{\mathcal{L}\mathcal{R}^2\mathcal{L}}$:

$$\eta_{\mathcal{L}\mathcal{R}^2\mathcal{L}}^{\ell} = \left\{ (a_\ell, a_r, \mu_\ell, \mu_r) \;\middle|\; \frac{\mu_\ell}{\mu_r} = -\frac{a_\ell^2 a_r^2 + a_\ell^2 a_r - a_\ell\, a_r + 1}{\left(a_\ell^2 a_r^2 - a_\ell\, a_r + a_\ell + 1\right) a_r} \right\} \tag{4.6}$$

$$\eta_{\mathcal{L}\mathcal{R}^2\mathcal{L}}^{r} = \left\{ (a_\ell, a_r, \mu_\ell, \mu_r) \;\middle|\; \frac{\mu_\ell}{\mu_r} = -\frac{\left(a_\ell^2 a_r^2 - a_\ell\, a_r + a r + 1\right) a_\ell}{a_\ell^2 a_r^2 + a_\ell\, a_r^2 - a_\ell\, a_r + 1} \right\} \tag{4.7}$$

Similarly, substituting these coefficients into the equations for $\eta_{\mathcal{L}\mathcal{R}^2\mathcal{L}}^{\ell/r}$ we obtain the equations for $\eta_{\mathcal{L}\mathcal{R}^2\mathcal{L}\mathcal{R}\mathcal{L}^2\mathcal{R}}^{\ell/r}$, and so on

$$\eta_{\mathcal{L}\mathcal{R}^2\mathcal{L}\mathcal{R}\mathcal{L}^2\mathcal{R}}^{\ell} = \left\{ (a_\ell, a_r, \mu_\ell, \mu_r) \;\middle|\; \frac{\mu_\ell}{\mu_r} = -\frac{a_\ell^5 a_r^4 - a_\ell^4 a_r^3 + a_\ell^3 a_r^3 + a_\ell^2 a_r - a_\ell\, a_r + 1}{\left(a_\ell^4 a_r^3 + a_\ell^3 a_r^3 - a_\ell^3 a_r^2 - a_\ell\, a_r + a_\ell + 1\right) a_r} \right\} \tag{4.8}$$

$$\eta_{\mathcal{L}\mathcal{R}^2\mathcal{L}\mathcal{R}\mathcal{L}^2\mathcal{R}}^{r} = \left\{ (a_\ell, a_r, \mu_\ell, \mu_r) \;\middle|\; \frac{\mu_\ell}{\mu_r} = -\frac{a_\ell^5 a_r^4 - a_\ell^4 a_r^3 + a_\ell^3 a_r^3 + a_\ell^2 a_r - a_\ell\, a_r + 1}{\left(a_\ell^4 a_r^3 + a_\ell^3 a_r^3 - a_\ell^3 a_r^2 - a_\ell\, a_r + a_\ell + 1\right) a_r} \right\} \tag{4.9}$$

$$\eta_{\mathcal{L}\mathcal{R}^2\mathcal{L}\mathcal{R}\mathcal{L}^2\mathcal{R}^2\mathcal{L}^2\mathcal{R}\mathcal{L}\mathcal{R}^2\mathcal{L}}^{\ell} = \left\{ (a_\ell, a_r, \mu_\ell, \mu_r) \;\middle|\; \frac{\mu_\ell}{\mu_r} = -\frac{N}{D} \right\} \tag{4.10}$$

$$\begin{aligned} N &= a_\ell^8 a_r^8 + a_\ell^8 a_r^7 - a_\ell^7 a_r^7 - a_\ell^6 a_r^5 + a_\ell^5 a_r^5 + a_\ell^5 a_r^4 - a_\ell^4 a_r^4 - a_\ell^4 a_r^3 + a_\ell^3 a_r^3 + a_\ell{}^2 a_r - a_\ell\, a_r + 1 \\ D &= \left(a_\ell^8 a_r^8 - a_\ell^7 a_r^7 + a_\ell^7 a_r^6 + a_\ell^5 a_r^5 - a_\ell^5 a_r^4 - a_\ell^4 a_r^4 + a_\ell^4 a_r^3 + a_\ell^3 a_r^3 - a_\ell^3 a_r^2 - a_\ell\, a_r + a_\ell + 1\right) a_r \end{aligned}$$

$$\eta_{\mathcal{L}\mathcal{R}^2\mathcal{L}\mathcal{R}\mathcal{L}^2\mathcal{R}^2\mathcal{L}^2\mathcal{R}\mathcal{L}\mathcal{R}^2\mathcal{L}}^{r} = \left\{ (a_\ell, a_r, \mu_\ell, \mu_r) \;\middle|\; \frac{\mu_\ell}{\mu_r} = -\frac{N}{D} \right\} \tag{4.11}$$

$$\begin{aligned} N &= \left(a_\ell^8 a_r^8 - a_\ell^7 a_r^7 + a_\ell^6 a_r^7 + a_\ell^5 a_r^5 - a l^4 a_r^5 - a_\ell^4 a_r^4 + a_\ell^3 a_r^4 + a_\ell^3 a_r^3 - a_\ell^2 a_r^3 - a_\ell\, a_r + a_r + 1\right) a_\ell \\ D &= a_\ell^8 a_r^8 + a_\ell^7 a_r^8 - a_\ell^7 a_r^7 - a_\ell^5 a_r^6 + a_\ell^5 a_r^5 + a_\ell^4 a_r^5 - a_\ell^4 a_r^4 - a_\ell^3 a_r^4 + a_\ell^3 a_r^3 + a_\ell\, a_r^2 - a_\ell\, a_r + 1 \end{aligned}$$

For increasing k the expressions for the crisis bifurcation curves $\eta_{\sigma_k}^{\ell/r}$ become too complicated to be presented here. However, in the special case of map (1.2) it is possible to generalize the results and to obtain the expressions for the crisis bifurcation curves caused by the unstable (2^k)-periodic orbits $\mathcal{O}_{\sigma_k}$ with arbitrary $k > 2$:

$$\eta_{\sigma_k}^{\ell/r} = \left\{ (a_\ell, a_r, \mu_\ell, \mu_r) \;\middle|\; \mu = \mp(-1)^k \frac{\left(a^{2^k} - 2\right)(a-1)^k}{\left(a^{2^{k-1}} + 1\right) a^{2^k}} \prod_{j=1}^{k-2} \left(a^{2^{k-2-j}} + 1\right)^j \right\} \tag{4.12}$$

The first 12 regions forming the bandcount doubling cascade within $\mathcal{Q}^3_{\mathcal{LR}}$ calculated by Eq. (4.12) are shown in Fig. 6. As one can see, the size of the regions decreases rapidly with increasing k. Recall that the last shown region has the bandcount 8191 and its boundaries are defined by the interior crisis bifurcation curves caused by an orbit with period 4096.

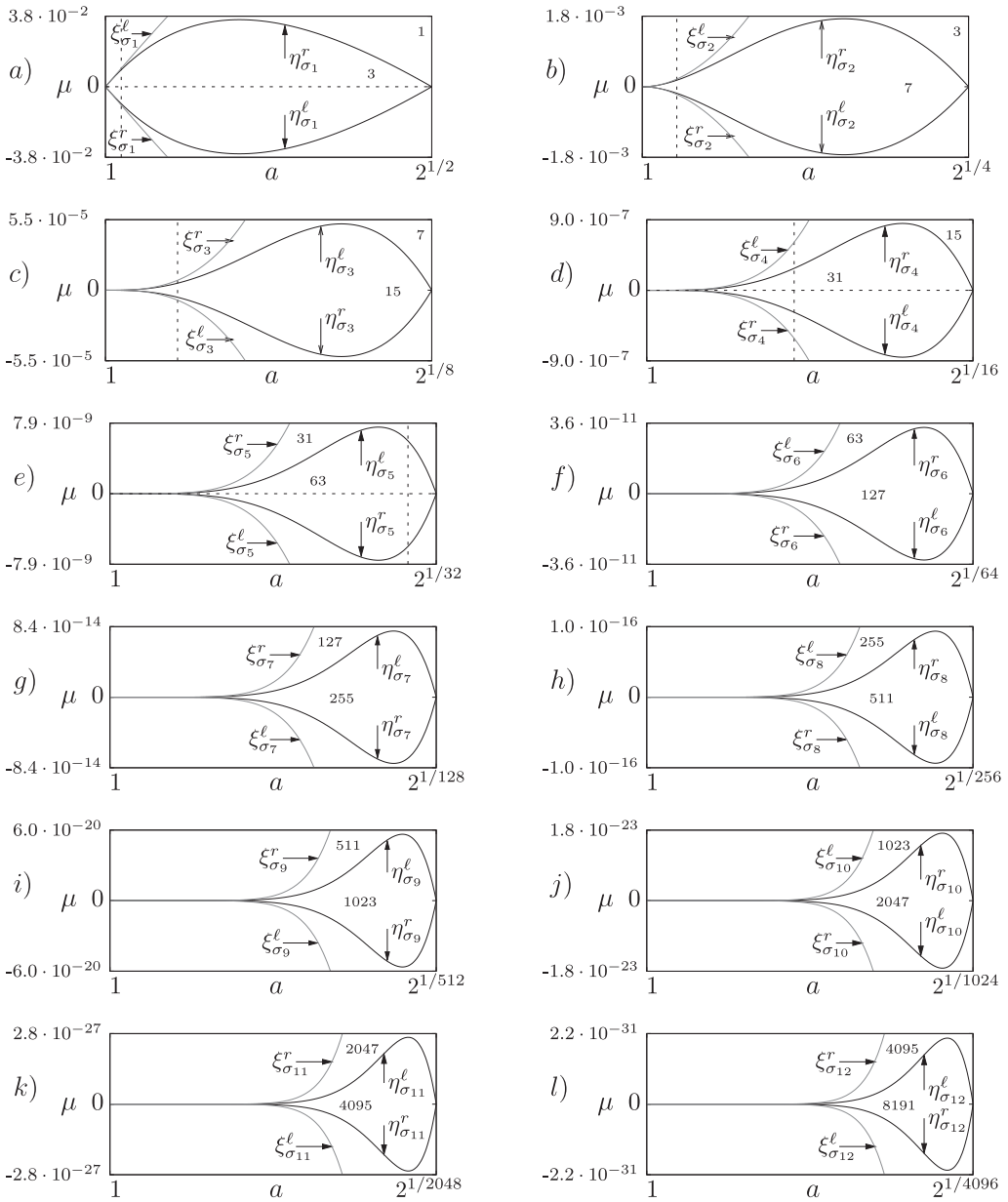

Fig. 6. Analytically calculated first twelve regions forming the bandcount doubling structure in map (1.2) within the region $\mathcal{Q}^3_{\mathcal{LR}}$. Small numbers in the figures refer to the bandcounts in the corresponding regions. Vertical dashed lines in figures *a*–*e* mark the value $a = 1.02$ which corresponds to the bifurcation scenario shown in Figs. 1b, 1d, 1f, and 1h. Horizontal dashed lines in figures (a)–(f) mark the line $\mu = 0$ and correspond to the bifurcation scenario shown in figures 5a–5f.

Now we can easily explain the situation regarding the self-similarity of the scenario shown in Fig. 1. As we already know, the region located in the middle of Fig. 1a is $\mathcal{Q}^3_{\mathcal{LR}}$. Its interior structure is shown enlarged in Fig. 1b. In the middle of this figure the region $\mathcal{Q}^7_{\sigma_2}$ is located, shown enlarged in Fig. 1d. Continuing this sequence of magnifications, Figs. 1f and 1h show the regions $\mathcal{Q}^{15}_{\sigma_3}$ and $\mathcal{Q}^{31}_{\sigma_4}$, respectively. In the middle of $\mathcal{Q}^{31}_{\sigma_4}$ the next region $\mathcal{Q}^{63}_{\sigma_5}$ can still be recognized, but if we

would consider the next magnification, no further sub-structures could be observed, similar to the situation in Fig. 1i. To explain that, consider Eq. (4.12) and Figs. 6a–e where the regions $\mathcal{Q}^3_{\sigma_1}, \ldots, \mathcal{Q}^{63}_{\sigma_5}$ are shown. As one can see, the most right point of the kth region is located at the line $\mu = 0$ and represents the intersection of the curves $\eta^{\ell}_{\sigma_k}$ and $\eta^{r}_{\sigma_k}$. From Eq. (4.12) we can easily see that this point is given by $\mu = 0$, $a^{2^k} = 2$, that means $a = 2^{1/2^k}$. As the value $a = 1.02$ used in Fig. 1 lies between $2^{1/64} \approx 1.010889$ and $2^{1/32} \approx 1.021897$, the region $\mathcal{Q}^{63}_{\sigma_5}$ will be intersected by the line $a = 1.02$ but not the region $\mathcal{Q}^{127}_{\sigma_6}$.

5. BANDCOUNT ADDING INSIDE $\mathcal{Q}^3_{\mathcal{LR}}$

As one can clearly see in Fig. 1, there are much more nested regions with higher bandcounts than we described above. In fact, it was already mentioned in [5] that within each region $\mathcal{Q}$ involved in a bandcount doubling cascade there is a complete bandcount adding structure originating from the same point where the region $\mathcal{Q}$ originates from. As an example, Fig. 7 shows the interior structure of the region $\mathcal{Q}^3_{\mathcal{LR}}$ in system (1.2) calculated numerically.

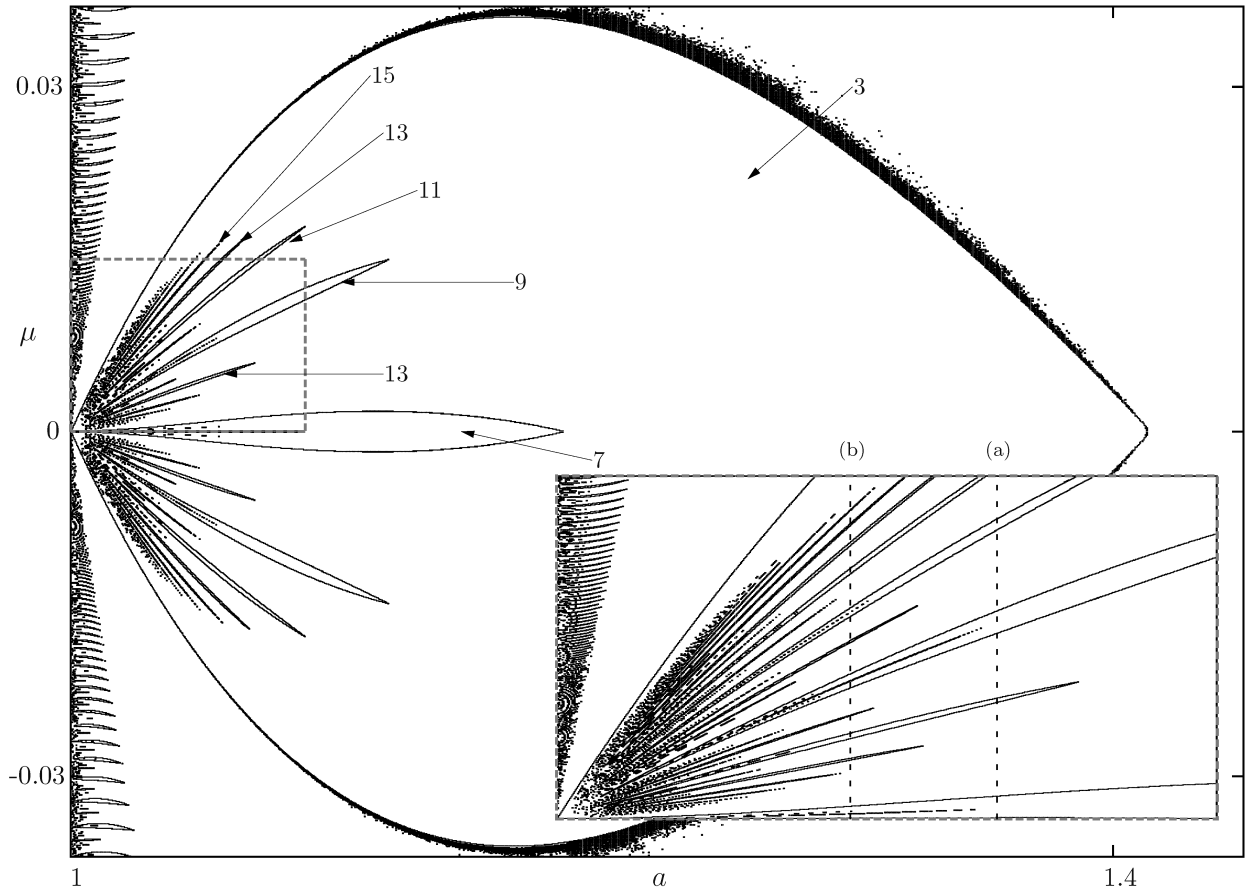

Fig. 7. Numerically calculated bandcount adding structure in map (1.2) within the region $\mathcal{Q}^3_{\mathcal{LR}}$. The marked rectangle is shown enlarged. Vertical lines marked with (a) and (b) correspond to Figs. 9 and 10, respectively.

As one can see, within the region $\mathcal{Q}^3_{\mathcal{LR}}$ we observe a complete bandcount adding structure originating from the big bang bifurcation point $a = 1$, $\mu = 0$. Typical bifurcation scenarios across this structure are shown Figs. 9 and 10, which correspond to the vertical lines marked in Figs. 7 and 8 with (a) and (b), respectively. It is clearly visible that for increasing bandcounts the corresponding regions in the parameter space become very narrow and are difficult to observe. Therefore, the question arises how the described structure can be calculated analytically. Fortunately, it turns out

that the replacement (4.3) is useful not only for the calculation of the bandcount doubling scenario in the middle part of the region $\mathcal{Q}^3_{\mathcal{LR}}$. By contrast, it can be used for the calculation of the complete bandcount adding structure within the region $\mathcal{Q}^3_{\mathcal{LR}}$. In [5] it was shown that the complexity level one of this structure is formed by interior crisis bifurcation curves of the orbits corresponding to the following two families of sequences

$$\{(\mathcal{LR})(\mathcal{RL})^n \mid n > 0\} \quad \text{and} \quad \{(\mathcal{RL})(\mathcal{LR})^n \mid n > 0\}. \tag{5.1}$$

It is not difficult to see that these sequences result from the sequences forming the first complexity level of the overall bandcount adding structure (see Eq. (3.1)) by the replacement (4.3). Therefore, there is no need for the intricate calculations of a few of the interior crisis bifurcation curves forming this structure nested in $\mathcal{Q}^3_{\mathcal{LR}}$ as presented in [5]. Instead, it is much more easy and convenient to substitute the coefficients $a_{\ell r}$, $\mu_{\ell r}$, $a_{r\ell}$, $\mu_{r\ell}$ given by Eqs. (4.5) into the equations for the crisis bifurcation curves $\eta^{\ell/r}_{\mathcal{LR}^{n_1}}$ and $\eta^{\ell/r}_{\mathcal{RL}^{n_1}}$ obtaining all crisis bifurcation curves involving the orbits corresponding to the sequences (5.1). For the curves $\eta^{\ell/r}_{(\mathcal{LR})(\mathcal{RL})^n}$ we get in this way

$$\eta^{\ell}_{(\mathcal{LR})(\mathcal{RL})^n} = \left\{ (a_\ell, a_r, \mu_\ell, \mu_r) \;\middle|\; \frac{\mu_\ell}{\mu_r} = -\frac{N}{D} \right\} \tag{5.2}$$

$$N = (a_\ell^3 a_r^2 - a_\ell^2 a_r + a_\ell a_r + a_\ell - 1)(a_\ell a_r)^{n+1} - 2a_\ell a_r(a_\ell^2 a_r - a_\ell + 1) + a_\ell^2 a_r^2 - a_\ell + 1$$

$$D = (a_\ell^2 a_r^2 + a_\ell a_r^2 - a_\ell a_r - a_r + 1)(a_\ell a_r)^{n+1} - 2a_\ell a_r(a_\ell a_r + a_r - 1) + a_\ell^2 a_r^3 + a_r - 1$$

$$\eta^{r}_{(\mathcal{LR})(\mathcal{RL})^n} = \left\{ (a_\ell, a_r, \mu_\ell, \mu_r) \;\middle|\; \frac{\mu_\ell}{\mu_r} = -\frac{N}{D} \right\} \tag{5.3}$$

$$N = (a_\ell a_r + a_\ell - 1)(a_\ell a_r)^{n+2} - 2a_\ell a_r(a_\ell - 1) - a_\ell^2 a_r^2 + a_\ell - 1$$

$$D = (a_\ell a_r^2 - a_r + 1)(a_\ell a_r)^{n+2} + 2a_\ell a_r(a_r - 1) - a_\ell^2 a_r^3 - a_r + 1$$

and the curves $\eta^{\ell/r}_{(\mathcal{RL})(\mathcal{LR})^n}$ result from $\eta^{\ell/r}_{(\mathcal{LR})(\mathcal{RL})^n}$ by exchanging ℓ and r. In Fig.8 both families of crisis bifurcation curves are shown for $n = 1 \ldots 20$.

The same procedure can be easily continued further. Using the same replacement (4.3) and the interior crisis bifurcation curves of complexity level two of the overall bandcount adding we obtain the interior crisis bifurcation curves of the complexity level two of the bandcount adding within $\mathcal{Q}^3_{\mathcal{LR}}$. It can be easily seen that the corresponding symbolic sequences are given by the families

$$\{\mathcal{LR}(\mathcal{RL})^{n_2}(\mathcal{RL}^2\mathcal{R}(\mathcal{RL})^{n_2})^{n_1}\} \tag{5.4}$$

$$\{\mathcal{RL}^2\mathcal{R}(\mathcal{RL})^{n_2}(\mathcal{LR}(\mathcal{RL})^{n_2})^{n_1}\} \tag{5.5}$$

and the two further families resulting from (5.4) and (5.5) by exchanging $\mathcal{L}$ and $\mathcal{R}$. The expressions of these bifurcation curves are too large to be presented here. Nevertheless, Fig. 8 shows the interior crisis bifurcation involving orbits corresponding to these families of orbits. Of course, the same calculation procedure can be continued for all further complexity levels.

To illustrate the obtained results let us consider the bifurcation structures along the lines marked with (a) and (b) in Figs. 7 and 8. The first of them (obtained for $a = 1.06$) is shown in Fig. 9. As one can see, in this case only three regions from the family $\mathcal{Q}^{2n+5}_{\mathcal{LR}(\mathcal{RL})^n}$ (complexity level one) are intersected within the considered interval of μ, namely $\mathcal{Q}^7_{\mathcal{LR}^2\mathcal{L}}$ $\mathcal{Q}^9_{\mathcal{LR}(\mathcal{RL})^2}$ and $\mathcal{Q}^{11}_{\mathcal{LR}(\mathcal{RL})^3}$. Additionally, one region of complexity level two, namely $\mathcal{Q}^{11}_{\mathcal{LR}^2\mathcal{LR}\mathcal{L}^2\mathcal{R}^2\mathcal{L}}$ is intersected. As one can see, Figs. 7 and 8 suggest that no further regions can be expected in the considered parameter interval, and Fig. 9 confirms that. However, it is also clear from Figs. 7 and 8 that for decreasing values of a more and more sub-regions with higher bandcounts appear in the bifurcation diagram. This can be seen in Fig. 10 ($a = 1.04$). The sequence of the regions of complexity level one continues in this case up to $\mathcal{Q}^{19}_{\mathcal{LR}(\mathcal{RL})^7}$. Note that this region is very narrow and can hardly be observed, but still exists. By contrast, the next region $\mathcal{Q}^{21}_{\mathcal{LR}(\mathcal{RL})^8}$ does not exist for the used value of a. Also, three further regions of the complexity level are shown in Fig. 10.

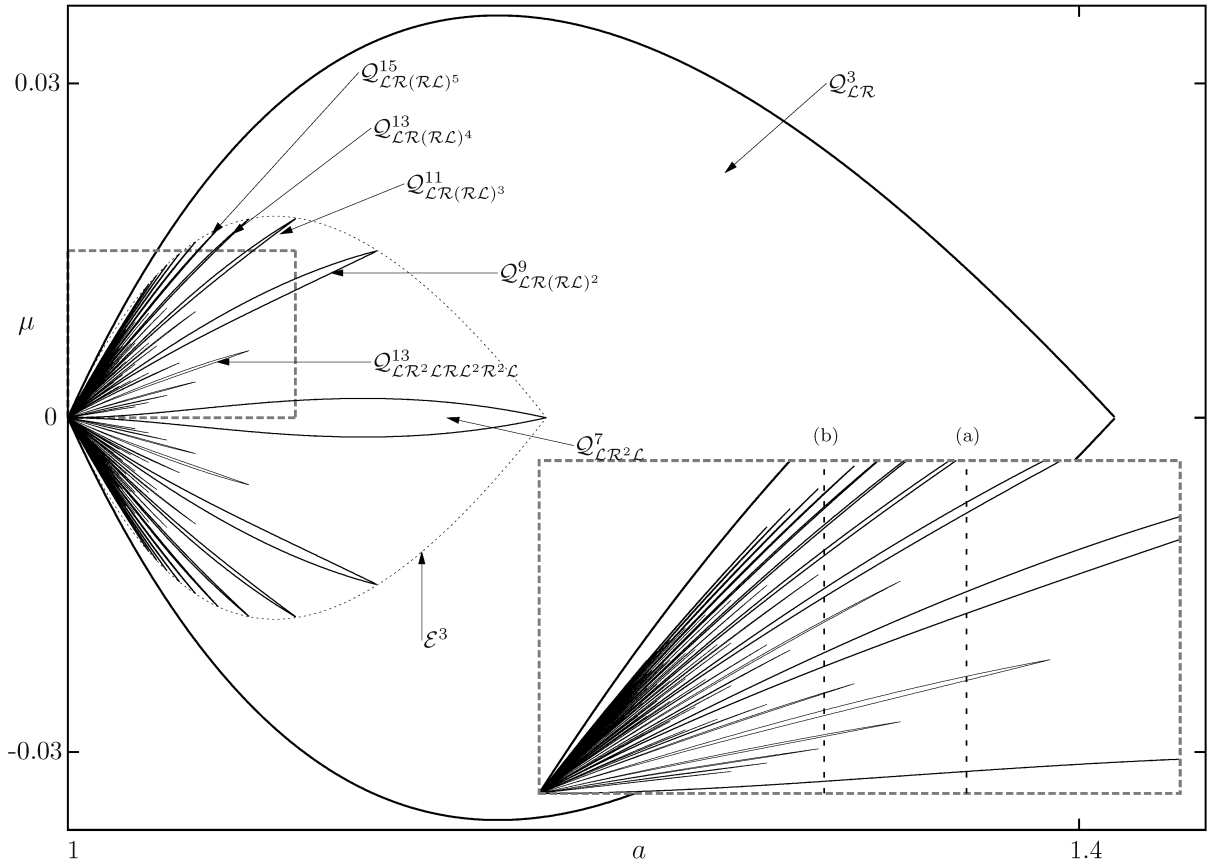

Fig. 8. Analytically calculated bandcount adding structure in map (1.2) within the region $\mathcal{Q}^3_{\mathcal{LR}}$. The bifurcation curves of the first two complexity levels are shown for $n_1 = 1..20$, $n_2 = 1..7$. The marked rectangle is shown enlarged. Vertical lines marked with (a) and (b) correspond to Figs. 9 and 10, respectively.

As one can see, also the calculation according to the replacement (4.3) can be interpreted as some kind of area-to-area mapping in the parameter space. In this case the overall bandcount adding structure will be mapped inside the region $\mathcal{Q}^3_{\mathcal{LR}}$. To be more precise, the area bounded by the line $a = 1$ and the envelope $\mathcal{E}^1$ will be mapped onto the area bounded by the envelope $\mathcal{E}^3$ marked in Fig. 8. Although both situations are very similar, let us emphasize a few differences between them. First, the replacements (3.7) and (3.8) contain n_1 as a parameter, hence the mapping defined by each of these replacements transforms one curve of a certain complexity level into an infinite family of curves in the next complexity level. By contrast, the replacement (4.3) is one-to-one: each curve from the overall bandcount adding structure will be mapped onto exactly one curve in the bandcount adding structure within the region $\mathcal{Q}^3_{\mathcal{LR}}$. Note additionally that the mapping defined by replacement (4.3) transforms the complete line $a = 1$ from $\mu = -1$ to $\mu = +1$ to one point $a = 1$, $\mu = 0$. Consequently, the image of each region of the overall bandcount adding structure originates now from this unique point.

Due to the self-similarity of the bandcount adding structure not only the region $\mathcal{Q}^3_{\mathcal{LR}}$ but also all other regions mentioned above contain nested sub-structures organized exactly in the same way as the overall bandcount adding structure. As an example let us consider the bandcount adding structure nested inside the region $\mathcal{Q}^7_{\mathcal{LR}^2\mathcal{L}}$ located in the middle of $\mathcal{Q}^3_{\mathcal{LR}}$. Therer the regions of complexity level one correspond to the sequences

$$\{(\mathcal{LR}^2\mathcal{L})(\mathcal{RL}^2\mathcal{R})^n\} \quad \text{and} \quad \{(\mathcal{RL}^2\mathcal{R})(\mathcal{LR}^2\mathcal{L})^n\} \tag{5.6}$$

for the complexity level two we have

$$\{(\mathcal{LR}^2\mathcal{L})(\mathcal{RL}^2\mathcal{R})^{n_2}((\mathcal{LR}^2\mathcal{L})(\mathcal{RL}^2\mathcal{R})^{n_2+1})^{n_1}\} \tag{5.7}$$

$$\{(\mathcal{LR}^2\mathcal{L})(\mathcal{RL}^2\mathcal{R})^{n_2+1}((\mathcal{LR}^2\mathcal{L})(\mathcal{RL}^2\mathcal{R})^{n_2})^{n_1}\} \tag{5.8}$$

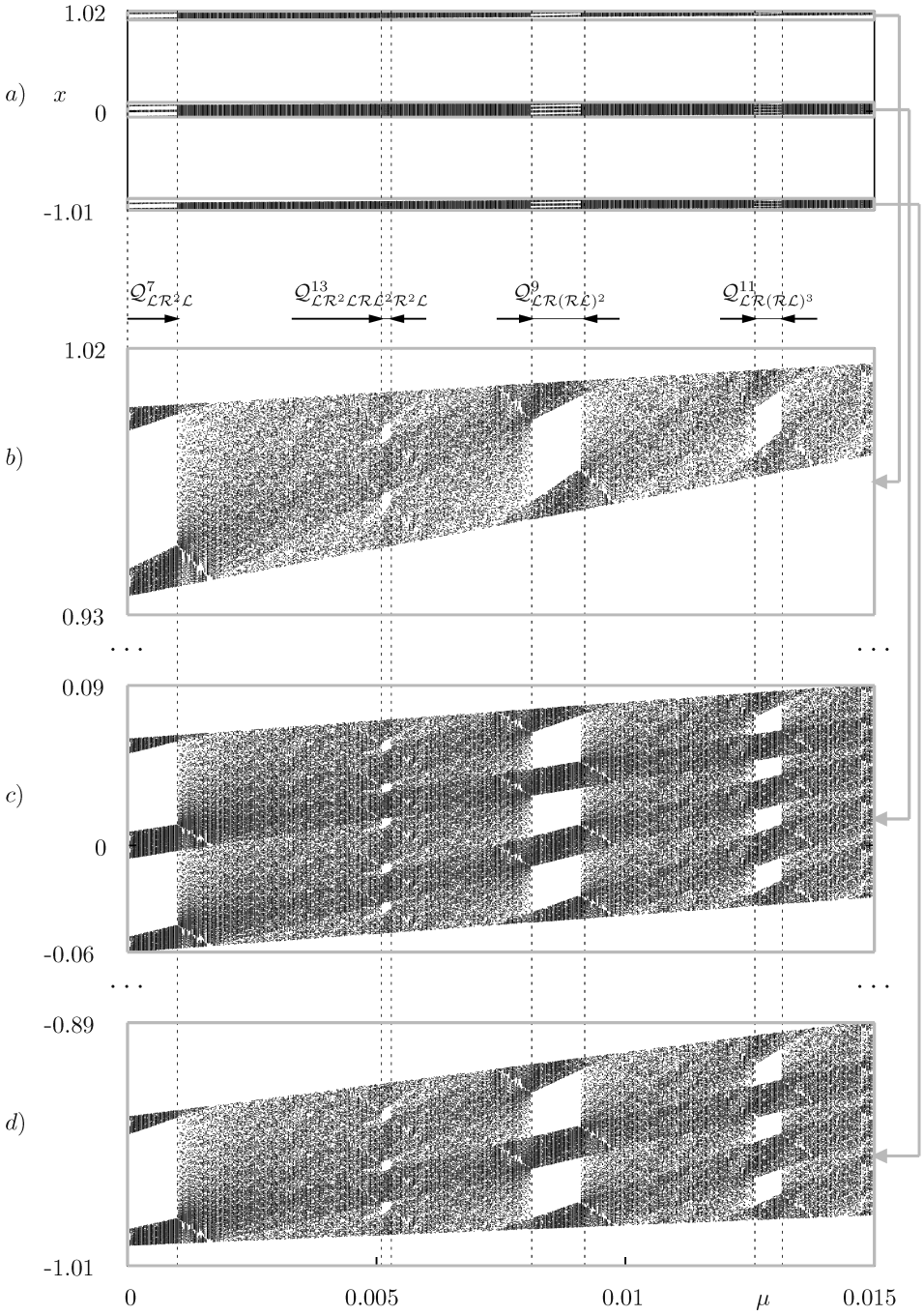

Fig. 9. Bifurcation structure along the line marked with (a) in Figs. 7 and 8. In (a) the complete bifurcation diagram is shown, in (b), (c), (d) the relevant parts are enlarged.

and the two further families resulting from (5.7) and (5.8) by exchanging the symbols $\mathcal{L}$ and $\mathcal{R}$. Note that there are two ways for the calculation of the corresponding bifurcation curves by the map replacement approach. The first one is to start with the bifurcation curves involved in the bandcount adding structure within the region $\mathcal{Q}^{3}_{\mathcal{LR}}$ and to use the replacement defined by Eq. (4.3). The second way is to start again with the bifurcation curves forming the overall bandcount adding structure. As one can see, in this case the following replacement must be used:

$$\mathcal{L} \to \mathcal{LR}^2\mathcal{L}, \qquad \mathcal{R} \to \mathcal{RL}^2\mathcal{L} \tag{5.9}$$

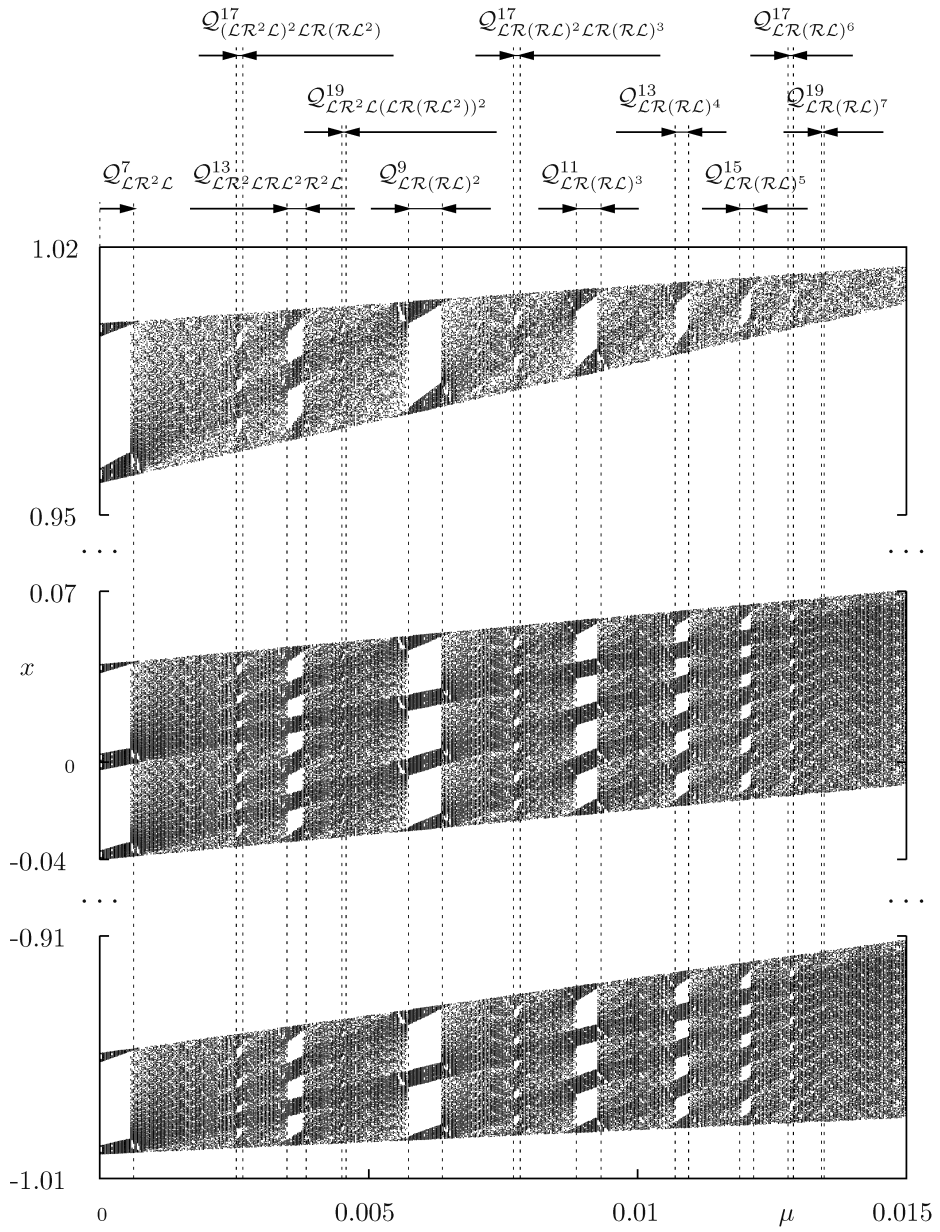

Fig. 10. Bifurcation structure along the line marked with (b) in Figs. 7 and 8.

Like the replacement defined by Eq. (4.3), also the replacement defined by Eq. (5.9) is one-to-one. In general, the bandcount adding structure within each of the regions involved in the bandcount doubling cascade described in Section 4 can be calculated similarly. The sub-structures within the region $\mathcal{Q}_{\sigma_i}^{1+2(2^i-1)}$ can be calculated either from the sub-structures in the region $\mathcal{Q}_{\sigma_i}^{1+2(2^{i-1}-1)}$ using the replacement defined by Eq. (4.3), or from the sub-structures of any other previous region using a corresponding more complex replacement.

6. SUMMARY

The idea behind the map replacement approach was initially reported in 1959 by Leonov [12–14]. In his works, the border-collision bifurcation curves forming the period-adding structure were calculated using one specific replacement. Later, in [11] we demonstrated how this approach can be used for the calculation of the border-collision bifurcation curves forming other bifurcation

scenarios. Furthermore we presented the rules how to find a replacement which allows to calculate the bifurcation curves for a given periodic orbit. In the current work we presented a next generalization step and demonstrate that the map replacement can also be used for the calculation of interior crisis bifurcation curves. It is shown that the bandcount adding structure formed by these bifurcations can be calculated using this approach in a very elegant and much more efficient way than using usual techniques. The fact that the calculation is done by a recursive procedure confirms the hypothesis regarding the self-similarity of the bandcount adding structure.

REFERENCES

1. Metropolis, N., Stein, M.L., Stein, P.R., On Finite Limit Sets for Transformations on the Unit Interval *J. Combinatorial Theory Ser. A*, 1973, vol. 15, pp. 25–44.
2. Mira, C., *Chaotic Dynamics*, World Scientific, 1987.
3. Banerjee, S., Yorke, J.A., and Grebogi, C., Robust Chaos, *Phys. Rev. Lett.*, 1998, vol. 80, no. 14, pp. 3049—3052.
4. Avrutin, V., Eckstein, B., and Schanz, M., On Detection of Multi-band Chaotic Attractors, *Proc. R. Soc. A*, 2007, vol. 463, no. 2081, pp. 1339–1358.
5. Avrutin, V. and Schanz, M., *Nonlinearity*, 2008, vol. 21, no. 5, pp. 1077–1103.
6. Gumowski, I. and Mira, C., *Dynamique chaotique, Transformations ponctuelles, Transitions. Ordre-désdordre*, Toulouse: Cepadues Éditions, 1980.
7. Mira, Ch., Gardini, L., Barugola, A., and Cathala, J.C., *Chaotic Dynamics in Two-Dimensional Nonivertible Maps*, World Sci. Ser. Nonlinear Sci. Ser. A Monogr. Treatises, vol. 20, River Edge, NJ: World Sci. Publ., 1996.
8. Fournier-Prunaret, D., Mira, C., and Gardini, L., Some Contact Bifurcations in Two-dimensional Examples, *Iteration Theory (ECIT 94), Opava*, Grazer Math. Ber., vol. 334, Graz: Karl-Franzens-Univ. Graz, 1997, pp. 77–96,.
9. Grebogi, C., Ott, E., and Yorke, J.A., Chaotic Attractors in Crisis, *Phys. Rev. Lett.*, 1982, vol. 48, no. 22, pp. 1507–1510.
10. Grebogi, C., Ott, E., and Yorke, J.A., Crises, Sudden Changes in Chaotic Attractors, and Transient Chaos *Physica D*, 1983, vol. 7, p. 181–200.
11. Avrutin, V., Gardini, L., and Schanz, M., Calculation of Bifurcation Curves by Map Replacement, *Int. J. Bifur. Chaos* (to appear).
12. N. N. Leonov, *Radiofisika*, 1959, V. 2, p. 942 (in Russian).
13. N. N. Leonov, *Radiofisika*, 1960, V. 3, p. 496 (in Russian).
14. N. N. Leonov, *Radiofisika*, 1960, V. 3, p. 872 (in Russian).